Thermal Nanofluid Property Model With Application to Nanofluid Flow in a Parallel-Disk System—Part I: A New Thermal Conductivity Model for Nanofluid Flow

ARTICLE *in* JOURNAL OF HEAT TRANSFER · MAY 2012

Impact Factor: 1.45 · DOI: 10.1115/1.4005632

2 AUTHORS:

Clement Kleinstreuer
North Carolina State University
272 PUBLICATIONS **7,432** CITATIONS

SEE PROFILE

Yu Feng
North Carolina State University
21 PUBLICATIONS **277** CITATIONS

SEE PROFILE

Thermal Nanofluid Property Model With Application to Nanofluid Flow in a Parallel-Disk System—Part I: A New Thermal Conductivity Model for Nanofluid Flow

Clement Kleinstreuer[1]
e-mail: ck@eos.ncsu.edu

Yu Feng

Department of Mechanical
and Aerospace Engineering,
North Carolina State University,
Raleigh, NC 27695-7910

This is a two-part paper, which proposes a new theory explaining the experimentally observed enhancement of the thermal conductivity, k_{nf}, of nanofluids (Part I) and discusses simulation results of nanofluid flow in a radial parallel-plate channel using different k_{nf}-models (Part II). Specifically, Part I provides the derivation of the new model as well as comparisons with benchmark experimental data sets and other theories, focusing mainly on aluminum and copper oxide nanoparticles in water. The new thermal conductivity expression consists of a base-fluid static part, k_{bf}, and a new "micromixing" part, k_{mm}, i.e., $k_{nf} = k_{bf} + k_{mm}$. While k_{bf} relies on Maxwell's theory, k_{mm} encapsulates nanoparticle characteristics and liquid properties as well as Brownian-motion induced nanoparticle fluctuations, nanoparticle volume fractions, mixture-temperature changes, particle–particle interactions, and random temperature fluctuations causing liquid-particle interactions. Thus, fundamental physics principles include the Brownian-motion effect, an extended Langevin equation with scaled interaction forces, and a turbulence-inspired heat transfer equation. The new model predicts experimental data for several types of metal-oxide nanoparticles ($20 < d_p < 50$ nm) in water with volume fractions up to 5% and mixture temperatures below 350 K. While the three competitive theories considered match selectively experimental data, their needs for curve-fitted functions and arbitrary parameters make these models not generally applicable. The new theory can be readily extended to accommodate other types of nanoparticle-liquid pairings and to include nonspherical nanomaterial. [DOI: 10.1115/1.4005632]

Keywords: nanofluids, thermal conductivity enhancement, new theory, data comparisons

1 Introduction

Of all the physical properties of nanofluids, i.e., dilute suspensions of typically metal-oxide nanoparticles in liquids, the thermal conductivity is the most intriguing one. The book by Das et al. [1] provides a state-of-the-art review of nanofluids, ranging from the manufacturing of nanoparticles to the experimental findings and property models of nanofluids. Other recent contributions, focusing on possible causes of enhanced thermal conductivity, are the papers by Tillman and Hill [2] analyzing the effect of an apparent liquid nanolayer surrounding nanoparticles, Li and Peterson [3] considering nanofluid temperature effects, Keblinski et al. [4] discussing the effect of chain-like particle clusters as well as others taking into account *p*H-values and dispersant concentrations. Clearly, experimental findings (see Fig. 1) have been controversial and theories did not fully explain the phenomenon of elevated thermal conductivity [1,5,6].

Thus, the objective is to derive a new theoretical model describing the mechanisms of effective thermal conductivity enhancement based on the micromixing concept for dilute mixtures, which is based on the Brownian motion of suspended nanoparticles in liquids. Specifically, the spherical particles increase the thermal conductivity of the mixtures (k_{static}), and random (Brownian) motion induces thermal dispersion (k_{mm}); hence, augmenting the energy exchange process. The latter can be considered as additional microscale mixing induced by chaotic nanoparticle motion. As a result, the effective thermal conductivity should be a function of particle size, temperature, particle volume fraction, and type of particle-liquid pairing.

Focusing on the Brownian-motion induced micromixing effect, Gupte and Advani [7] proposed a numerical approach (i.e., unit cell approach) to calculate the free-fall velocities of uniformly distributed micron particles, induced heat-transfer effects. Their approach for calculating the particles' velocity field was helpful for developing theories later on. Other papers dealing with heat-transfer effects induced by micron particle motion (including rotation) were reviewed by Leal [8] and Gupte et al. [9].

Several papers claimed that the Brownian-motion effect contributes very little to the thermal conductivity enhancement of nanofluids. Relying on the results of Leal [8] and Gupte et al. [9], Wang et al. [10] claimed that the effective thermal conductivity enhancement due to Brownian motion (including rotation) is trivial. In addition, by comparing the Brownian particle diffusion time scale and heat-transfer time scale, Keblinski et al. [4] concluded that the amount of heat transferred by Brownian particle diffusion contributed little to the thermal conductivity enhancement. However, Wang et al. [10] and Keblinski et al. [4] failed to consider the surrounding fluid motion induced by the nano particles, which is the essence of micromixing and hence k_{nf}-enhancement.

[1]Corresponding author.

Contributed by the Heat Transfer Division of ASME for publication in the JOURNAL OF HEAT TRANSFER. Manuscript received April 5, 2010; final manuscript received November 5, 2010; published online April 11, 2012. Assoc. Editor: Ping Cheng.

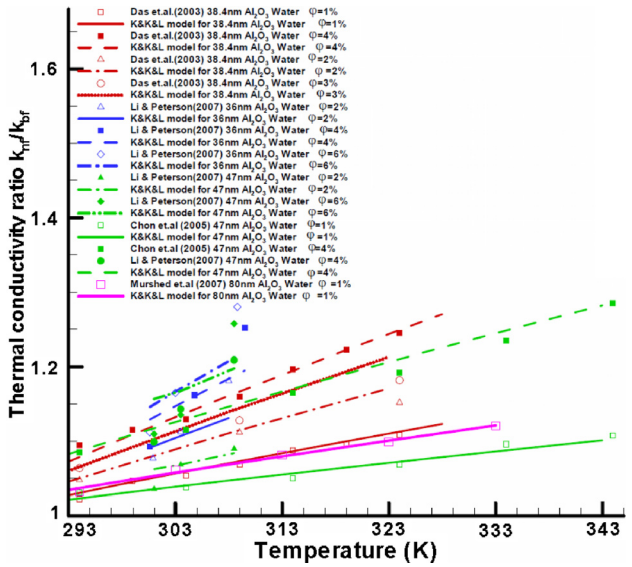

Fig. 1 Comparison between KKL model and benchmark experimental data

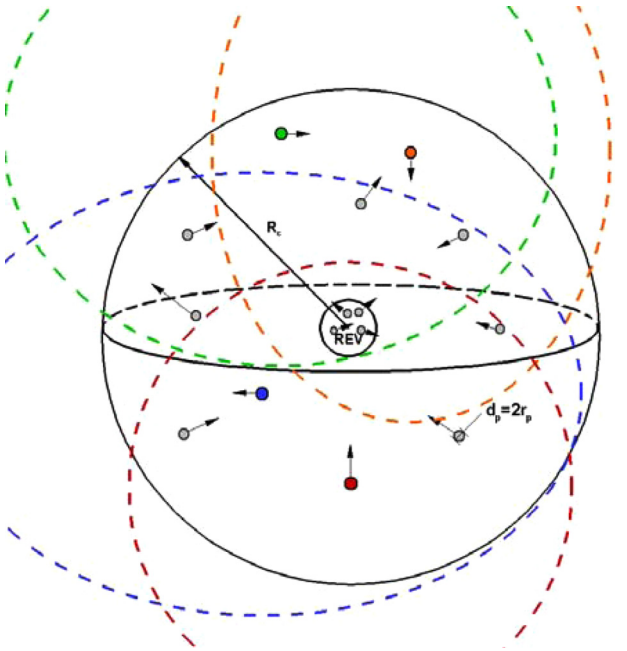

Fig. 2 Sketch for multinanoparticle Brownian-motion influence on base fluid

One of the competitive theories for k_{eff}, i.e., the Koo–Kleinstreuer–Li (KKL) model [6], relies on the Brownian-motion induced micromixing concept and is a point of departure for the new theory. However, the KKL model has several shortcomings: (i) it is two-dimensional, neglecting the asymmetric diffusion caused by Brownian motion; (ii) it was assumed that the surrounding fluid will move with the particle at a uniform velocity; (iii) temperature effects were encapsulated via a curve-fitted function; and (iv) interaction between nanoparticles was neglected. The new model, labeled Feng-Kleinstreuer (F-K) model, improves on these aspects, using a statistical method to take the particle–-particle interaction into account, solves the Reynolds-averaged heat transfer equation, treats the fluctuation velocity as a function of the distance between particle and "fluid package," and superimposes the induced fluctuation velocities to realize multiparticle effects. Other k_{nf}-theories considered in this paper are the multisphere-Brownian (MSB) model of Prasher [11] and the model by Bao [12]. Inspired by thermal flow in porous media [13], Xuan and Roetzel [14] proposed intrinsic phase averaging of a nanofluid's velocity and temperature fields. Specifically, they described the nanoparticle-induced perturbation via a dispersion parameter, while they employed for k_{eff} the Maxwell correlation.

2 Theory

The objective is to describe, based on sound physics, the convective heat transfer of dispersed spherical nanoparticles in dilute liquid-based suspensions. Deriving the needed thermal conductivity of such nanofluids requires a number of assumptions, which have been summarized in Table 1 and further justified throughout this section.

2.1 Parameter Decompositions. Enlightened by the turbulence concept, i.e., just random quantity fluctuations, which can cause additional fluid mixing and not turbulence structures such as diverse eddies, an analogy is made between random Brownian-motion generated fluid-cell fluctuations and turbulence. Thus, the Reynolds decomposition of velocity and temperature can be expressed as follows:

$$\vec{v}_{nf} = \bar{\vec{v}}_{nf} + \vec{v}'_{nf} \tag{1a}$$

$$\vec{v}_p = \vec{v}'_p \tag{1b}$$

$$T = \bar{T} + T' \tag{1c}$$

where superscript $'$ represents the fluctuation terms and $\bar{}$ represents the time-averaged terms. One may notice that the nanofluid fluctuation velocity is induced by the nanoparticle's relative fluctuation velocity $\vec{v}'_p$, generated by the Brownian motion. By definition, time-averaged fluctuation variables are zero, i.e.

$$\overline{\vec{v}'_{nf}} = \overline{\vec{v}'_p} = \overline{T'} = 0 \tag{2}$$

2.2 Mechanisms. As implied, the anomalous enhancement of thermal conductivity in nanofluids is due to the Brownian motion and interactions of nanoparticles. A schematic of the microstructure of a nanofluid is shown in Fig. 2. Simplified versions of the general case are depicted in Figs. 3 and 4. The latter depicts the details of the rectangular dashed-line region in Fig. 3.

Table 1 Main assumptions and brief justifications for F-K model derivation

Assumption	Brief justification	Equation
Reynolds decomposition for Brownian-motion induced particle velocities	Instantaneous nanoparticle velocity contains also a random term similar to the random velocity in turbulence	Eq. (1)
Prandtl's mixing length theory for Brownian-motion induced temperature fluctuations	It is most appropriate for the Brownian-motion induced temperature fluctuation term because the mixing length theory has been derived based on concepts from kinetic theory	Eq. (27)
Linear correlation for interactions between particles	For obtaining an analytical solution, it is necessary to simplify the nonlinear correlation	Eq. (29)

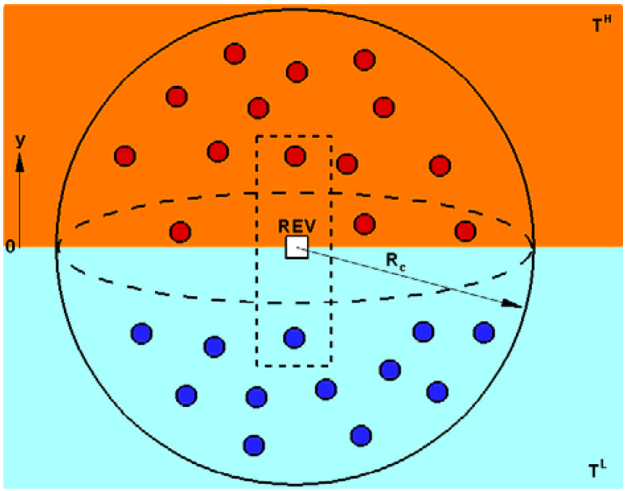

Fig. 3 Sketch for capturing sphere around fluid package

Because of the low particle Reynolds numbers involved, the analytical solution for Stokes flow around a spherical particle can be employed [15]. Specifically, the relative motion between particles and their surrounding fluid package will generate an induced fluid velocity, which will increase the intensity of the micromixing effects between higher fluid temperature and lower temperature fields, thereby enhancing the thermal conductivity of moving nanofluids [16]. Additionally, as incorporated in classical models, the mixture properties affected by the nanoparticles contribute to the enhancement of the thermal conductivity. Another part of the induced fluctuation velocity of the nanofluid is due to the base fluid's molecular thermal fluctuations which cannot be neglected; because if the nanofluid is stationary, the average velocity of the nanofluid is considered to be zero. In order to encapsulate all contributions, the thermal conductivity of the nanofluid, k_{nf}, is divided into two parts

$$k_{nf} = k_{static} + k_{mm} \tag{3}$$

where k_{static} is the base-fluid thermal conductivity part, while k_{mm} is the micromixing thermal conductivity part. We propose that the anomalous enhancement is due to the particle-liquid and particle–particle interactions as well as the particle and liquid thermal properties.

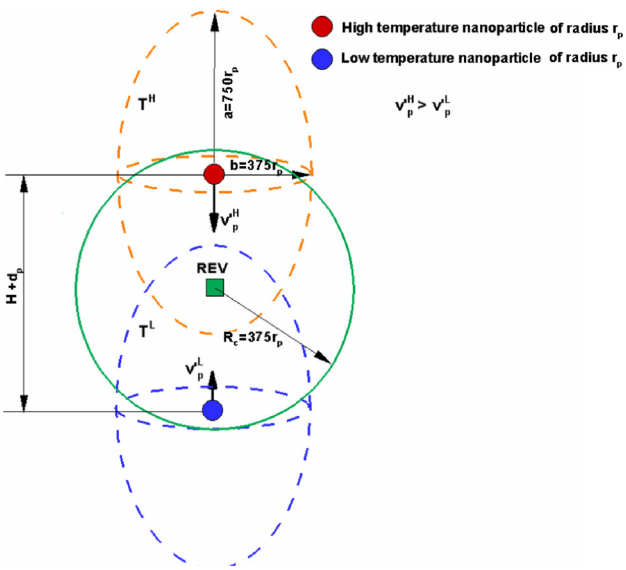

Fig. 4 Sketch for induced velocities due to nanoparticles at different temperatures

2.3 Base Fluid and Particle Interaction

2.3.1 Induced Fluid Velocity of Nanofluids by Particle Motion. In our investigation, the induced velocity of an ellipsoidal fluid package due to nanoparticle fluctuations can be written as [15]

$$v_{nf}^{(r)\prime} = -2\left(\frac{\left|\vec{v}_p'\right| r_p^{\,3}}{4r^3} - 3\frac{\left|\vec{v}_p'\right| r_p}{4r}\right)\cos\theta \tag{4a}$$

$$v_{nf}^{(\theta)\prime} = -\left(\frac{\left|\vec{v}_p'\right| r_p^{\,3}}{4r^3} + 3\frac{\left|\vec{v}_p'\right| r_p}{4r}\right)\sin\theta \tag{4b}$$

$$v_{nf}^{(\phi)\prime} = 0 \tag{4c}$$

where r_p is the nanoparticle radius (see Fig. 3). Clearly, the range of r is naturally limited, i.e., $r_p \le r \le r_c$, where r_c is the radius of influence (see Eq. (6)).

Neglecting higher-order terms, the induced velocity magnitude $\left|\overrightarrow{v'_{nf}}\right|$ can be written as

$$\left|\overrightarrow{v'_{nf}}\right| = \sqrt{\left(\frac{3}{2}\frac{r_p}{r}\cos\theta\right)^2 + \left(\frac{3}{4}\frac{r_p}{r}\sin\theta\right)^2}\left|\vec{v}_p\right| = \frac{3}{4}\frac{r_p}{r}\sqrt{(3\cos^2\theta+1)}\left|\vec{v}_p\right| \tag{5a,b}$$

We define the radius of influence r_c for a nanoparticle based on the assumption that at $r = r_c$ $\left|\overrightarrow{v'_{nf}}\right| = 0.2\% \cdot \left|\vec{v}_p\right|$, which is the 99.8% criterion. Thus, r_c can be expressed as

$$r_c = 375 r_p \sqrt{(3\cos^2\theta + 1)} \tag{6}$$

Equation (5) implies an ellipsoidal fluid package, which indicates that the nanoparticle can influence surrounding fluid of ellipsoidal shape with $a = r_c(\theta = 0) = 750 r_p$ (long axis) and $b = r_c\left(\theta = \frac{\pi}{2}\right) = 375 r_p$ (short axis). One should notice that the long axis extends in the direction of the nanoparticle fluctuation velocity. Hence, based on $r_c\left(\theta = \frac{\pi}{2}\right)$, we define the capture radius of a spherical fluid package as (see Fig. 2)

$$R_c = 375 r_p \tag{7}$$

That assures that any nanoparticle has a distance less than R_C to the fluid package, which an induced velocity of at least $0.2\% \cdot \left|\vec{v}_p\right|$. However, Eq. (7) will restrict the micromixing effect because some nanoparticles can also induce velocities larger than $0.2\% \cdot \left|\vec{v}_p\right|$, i.e., in the region between $375 r_p < r \le 750 r_p$, which is addressed later on. The area of influence is shown in Fig. 2 via colored dashed elliptical curves.

This defines a spherical fluid package, which is small enough to be considered a "point" from a macroscopic view, i.e., forming a homogeneous continuum. In well-dispersed suspensions, the nanoparticles are distributed axisymmetrically by the sphere-of-influence for the fluid package (see Fig. 3). Here, the induced velocity of nanofluids is only due to the temperature difference (see Figs. 3 and 4) in the sphere-of-influence which produces different velocity magnitudes due to Brownian motion. This is further discussed in Sec. 5.2, see Eq. (35), which shows the temperature dependence of the nanoparticle fluctuation velocity. Such a relationship between velocity and temperature can be interpreted from a physical view-point as follows. The particle surrounded by a higher temperature fluid will

have a higher average fluctuation velocity, $v_p' \sim \sqrt{\kappa_B T/(2m_p)}$, in any direction [17]; as a result, higher average fluctuation velocities of particles induce a higher fluctuation velocity of the fluid package. Therefore, if two representative nanoparticles in difference temperature regions (see Fig. 4) co-influence a fluid package at the center of them, a "drift velocity" is produced for the fluid package with a direction opposite to the gradient of temperature. The drift velocity may also cause an enhancement of diffusion due to temperature gradients. Without loss of generality, the drift velocity is generated in well-dispersed multi-nanoparticle structure around a fluid package (see Fig. 3).

For the capturing sphere (Fig. 3), being very small compared to the macroscale, it can be assumed that the higher temperature region is characterized by a uniform temperature T^H and a lower temperature region with T^L. Such a simplification for the temperature field is necessary and reasonable in order to calculate the thermally induced velocity of nanofluids. Clearly, the fluid package is small so that the local temperature difference is small, and using a truncated Taylor series for T^H in terms of T^L, the local temperature gradient can be expressed as

$$\frac{\partial \overline{T}}{\partial y} = \frac{T^H - T^L}{R_c} \tag{8}$$

We consider only the effect induced by nanoparticles (i.e., Brownian motion) and assume that the suspension is well dispersed. By integrating over the sphere-of-influence, the magnitude of the induced velocity in the y-direction can be calculated as (see Figs. 2 and 5)

$$v_{nf}^{(y)'} = \frac{\varphi}{\frac{4\pi r_p^3}{3}} \int_0^{2\pi} \int_0^{\frac{\pi}{2}} \int_{\frac{H}{2}}^{R_c} r^2 \left(\left(v_{nf}^{(r)/H} - v_{nf}^{(r)/L} \right) \cdot \cos\theta + \left(v_{nf}^{(\theta)/H} - v_{nf}^{(\theta)/L} \right) \cdot \sin\theta \right) dr d\theta d\phi \tag{9}$$

where the coefficient $\varphi/\left(4\pi r_p^3/3\right)$ was enlarged for nanoparticle volume nondimensionalization. Substituting Eq. (4*a*), we obtain

$$v_{nf}^{(y)'} = \left(\left| v_p' \right|^H - \left| v_p' \right|^L \right) \cdot \frac{3}{2} \varphi \left(\frac{3}{32} \pi \frac{R_c^2}{r_p^2} - \frac{3}{128} \pi \frac{H^2}{r_p^2} - \frac{3\pi}{256} \ln(R_c) - \frac{3\pi}{256} \ln 2 \right) \tag{10}$$

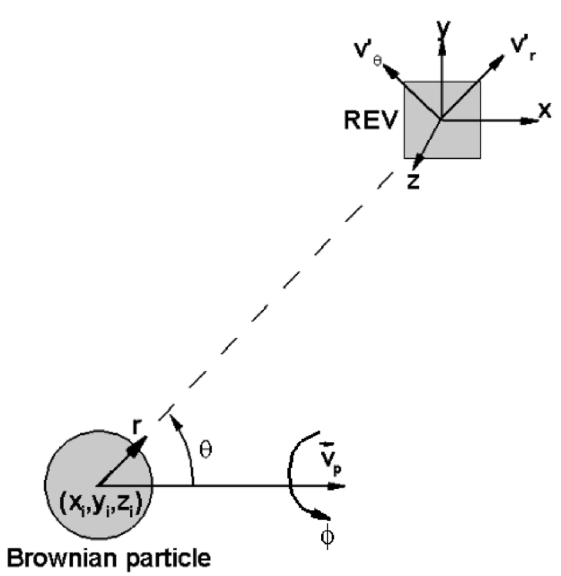

Fig. 5 Spherical coordinates and Cartesian coordinates for calculating Stokes flow around a particle

where H is the distance between two nanoparticles, which can be expressed as a function of volume fraction φ (see Fig. 4)

$$H = \sqrt[3]{\frac{\pi d_p^3}{6\varphi}} - d_p \tag{11}$$

2.3.2 Brownian-Motion Induced Particle Velocity. Brownian motion of nanoparticles is due to collisions between base-fluid molecules and nanoparticles. Brownian motion is independent of the source of motion of other particles. We can express the Brownian-motion velocity of a nanoparticle in Cartesian coordinates as

$$\vec{v}_p^{\,BM} = (\xi, \eta, \chi) \sqrt{\frac{\kappa_B T}{2m_p}} \tag{12}$$

where $\kappa_B = 1.3806503 \times 10^{-23}$ m^2 kg s^{-2} K^{-1} is the Boltzmann constant, $m_p = \frac{4}{3}\pi r_p^3$ is the nanoparticle mass, and (ξ, η, χ) are three random numbers satisfying a normal distribution

$$p(x) = \frac{1}{\sqrt{2\pi}} \exp\left(-\frac{x^2}{2} \right) \quad x \in (-\infty, \infty) \tag{13}$$

2.4 Forces Acting on Nanoparticles

2.4.1 Random Force. Clearly, the Brownian-motion effect can be expressed in terms of a force $\vec{F_B}(t)$. That force causes a random velocity as expressed in Eq. (12).

2.4.2 Stokes Force. For nanoparticles moving in a base fluid, not only the base-fluid molecules collide with the particles to transfer kinetic energy to them but also dissipate the kinetic energy of the particle by frictional (i.e., drag) force. For $Re \leq 1.0$, the drag (Stokes) force is [15]

$$\vec{F}_{Stokes} = 3\pi \vec{v}_p' d_p \mu_{bf} \tag{14}$$

Based on the co-effects of Stokes force and Brownian-motion force, the nanoparticles characteristic time for Brownian motion can be stated as [12,18]

$$\tau_p = \frac{m_p}{3\pi \mu_{bf} d_p} \tag{15a}$$

Actually, Eq. (15*a*) results from the momentum/impulse balance

$$m_p v = F_{Stokes} \tau_p \tag{15b}$$

In a very short time interval τ_p, assuming v is constant, τ_p provided by Eq. (15*a*) indicates the time interval during which the particle can maintain its original velocity.

2.5 Particle–Particle Interaction. Although we focused on *dilute* suspensions, where nanoparticle displacements satisfy Gaussian distribution, the average distance between two nanoparticles in such a mixture is not that large. For example, for a suspension with a 4% volume fraction of 47 nm diameter Al_2O_3 nanoparticles, the average distance between two particles is 174 nm. That makes the van der Waals force and electrostatic repulsion force between particles measurable. Thus, the energy redistribution due to nanoparticle interactions will contribute to the enhancement of thermal conductivity. Similar views were expressed by Keblinski et al. [4] and Wang and Xu [19]. Thus, for the theoretical analysis of two-nanoparticle interaction, the van der Waals force is considered [20].

2.5.1 London Dispersion Force. Dispersion resulting from interactions between nanoparticles is basically captured by the

Derjaguin–Landau–Verwey–Overbeek (DLVO) theory [18]. DLVO theory combines the effects of van der Waals and double layer forces. The attraction forces can be generally named as van der Waals force [18], which is defined as the attraction between molecules, other than covalent bonds or the electrostatic interaction of ions. The van der Waals force combines the permanent dipole-permanent dipole force, permanent dipole-induced dipole force, and dispersion force. It can be divided into three categories: orientation force, induction force, and dispersion force. For neutral molecules or particles, the orientation force and induction force can be neglected. Thus, only the dispersion force, which is an interaction between induced-dipole and induced-dipole need to be considered. Such a force is also known as the London dispersion force.

The London dispersion potential ψ_{LD} for two identical nanoparticles can be written as [18]

$$\psi_{LD} = -\frac{A_{pbp} d_p}{6H}\left[\frac{2d_p}{H+2d_p} + \frac{2Hd_p}{(H+d_p)^2} + \frac{4H}{d_p}\ln\left(2H\cdot\frac{H+2d_p}{(H+d_p)^2}\right)\right] \tag{16}$$

If $d_p \ll H$, Eq. (16) can be simplified to

$$\psi_{LD} = -\frac{A_{pbp} d_p}{24H} \tag{17}$$

where $H + d_p$ is the distance between mass centers of the two particles at equilibrium position which is given as Eq. (11). The parameter A_{pbp} is the Hamaker constant [34] between two identical particles (p) dispersed in a base fluid (b). For Al_2O_3 − water nanofluids, $A_{pbp} = 4.17 \times 10^{-20}$ J. Considering Eqs. (16) and (17), it is noticed that the interaction between particles is $O(H^{-2})$, which demonstrates that the van der Waals force cannot be easily neglected.

2.5.2 Electrostatic Repulsion Force. The electrostatic repulsion potential stems from the overlap of the electric double layers (EDL) around the nanoparticles when they are close to each other. The repulsion force is a short-distance force of which the potential can be written as [18]

$$\psi_{Rep} = \Lambda \cdot 32\pi d_p \kappa_B T \kappa^{-2} \rho_{el} \tanh^2\left(\frac{\sigma e \phi_0}{4\kappa_B T}\right)\exp(-\kappa h) \tag{18}$$

where κ_B is the Boltzmann constant, σ is the valency of the ions, κ is the Debye constant which is the inverse of the Debye length, ρ_{el} is the concentration of electrons, and ϕ_0 is the EDL-potential at the surfaces of the nanoparticles. Because the above expression for ψ_{Rep} is suitable for $\kappa d_p > 10$, we introduce Λ as an adjustment constant for nanoparticles where κ^{-1} and d_p is of the same order of 1×10^{-9}, so that the condition $\kappa d_p > 10$ cannot be guaranteed. In reality, $\kappa d_p < 4$ for metal-oxide nanofluids (e.g., Al_2O_3-water) and metal nanofluids (i.e., Cu-water, Ag-water, and Au-water) [21]. Another expression for ψ_{Rep} can be obtained via the Lennard–Jones potential [22], which is used in Sec. 3.

2.6 Particle-Basefluid Interaction. As mentioned, the fluctuation velocity of the nanofluid is not only induced by the nanoparticles' Brownian motion but also by the thermal fluctuations of the surrounding base-fluid molecules. The Brownian motion contributes to the enhancement of micromixing thermal conductivity part. The induced fluctuation velocity by a base-fluid molecule of distance r can be expressed as [15]

$$v_{nf}^{(r)\prime} = -2\left(\frac{\sqrt{\frac{\kappa_B \overline{T}}{2m_{bf}}}r_p^{\,3}}{4r^3} - 3\frac{\sqrt{\frac{\kappa_B \overline{T}}{2m_{bf}}}r_p}{4r}\right)\cos\theta \tag{19a}$$

$$v_{nf}^{(\theta)\prime} = -\left(\frac{\sqrt{\frac{\kappa_B \overline{T}}{2m_{bf}}}r_p^{\,3}}{4r^3} + 3\frac{\sqrt{\frac{\kappa_B \overline{T}}{2m_{bf}}}r_p}{4r}\right)\sin\theta \tag{19b}$$

$$v_{nf}^{(\phi)\prime} = 0 \tag{19c}$$

where the term $\sqrt{\frac{\kappa_B \overline{T}}{2m_{bf}}}$ represents the thermal velocity of the base-fluid molecules, while m_{bf} is the mass of the base-fluid molecule.

3 Relative Order-of-Magnitude Analysis for Forces

Applying a relative order-of-magnitude analysis (ROMA) to the forces considered for nanofluids, i.e., London dispersion force, electrostatic repulsion force, and Stokes force, some simplifications can be made. In light of Eqs. (14) and (17) as well as the Lennard–Jones potential [22] for dilute nanofluids, the focus is on $\varphi = 4\%$ of Al_2O_3-water nanofluid with nanoparticle diameter 47 nm, as a sample application. ROMA yielded $F_{LD} \sim O(2.7 \times 10^{-14}$ N), $F_{Rep} \sim F_{LD}$ and $F_{Stokes} \sim O(5.8 \times 10^{-12}$ N), for two-particle interaction, which appears to be very small. However, the prevailing multiparticle interactions cannot be neglected and hence the magnitude of F_{LD} is multiplied by a correlation (see Sec. 6.1) factor C_c. Therefore, $F_{LD} \sim O(1.9 \times 10^{-12}$ N) which is of the same order as $F_{Stokes} \sim O(5.8 \times 10^{-12}$ N) so that even in diluted nanofluids all forces should be considered.

4 Governing Equations

For nanofluids, properties such as μ, c_p, and ρ, are dependent on temperature and volume fraction; hence, the governing equations are written as follows:

$$\text{Continuity equation: } \nabla \cdot (\rho \vec{v})_{nf} = 0 \tag{20}$$

$$\text{Momentumequation: } \frac{\partial \vec{v}_{nf}}{\partial t} + \vec{v}_{nf} \cdot \nabla \vec{v}_{nf} = -\frac{\nabla p}{\rho_{nf}} + \mu_{nf} \nabla^2 \vec{v}_{nf} \tag{21}$$

$$\text{Energy equation: } \frac{\partial T}{\partial t} + \nabla \cdot (\vec{v}_{nf} T) = \nabla \cdot \left[\left(\frac{k_{nf}}{(\rho c_p)_{nf}}\right)\nabla T\right] + \frac{\Phi}{(\rho c_p)_{nf}} \tag{22}$$

where the viscous dissipation function Φ is given as

$$\Phi = 2\mu_{nf}\left[\left(\frac{\partial v_{nf}^{(x)}}{\partial x}\right)^2 + \left(\frac{\partial v_{nf}^{(y)}}{\partial y}\right)^2 + \left(\frac{\partial v_{nf}^{(z)}}{\partial z}\right)^2\right] + \mu_{nf}\left[\left(\frac{\partial v_{nf}^{(x)}}{\partial y} + \frac{\partial v_{nf}^{(y)}}{\partial x}\right)^2 + \left(\frac{\partial v_{nf}^{(z)}}{\partial z} + \frac{\partial v_{nf}^{(x)}}{\partial x}\right)^2 + \left(\frac{\partial v_{nf}^{(z)}}{\partial y} + \frac{\partial v_{nf}^{(y)}}{\partial z}\right)^2\right] \tag{23}$$

Based on Newton's second law of motion, nanoparticle fluctuations can be expressed in terms of the extended Langevin equation

$$m_p \frac{d\vec{v}_p'}{dt} = -\nabla(\Psi_{LD} + \Psi_{Rep}) - \vec{F}_{Stokes} + \vec{F}_B(t) \tag{24}$$

where $\Psi_{LD} = \sum_i \psi^i{}_{LD}$ and $\Psi_{Rep} = \sum_i \psi^i{}_{Rep}$, which are representing the total London dispersion potential and total electrostatic repulsion potential. Expressions for $\psi^i{}_{LD}$ and $\psi^i{}_{Rep}$ are given in Eqs. (16) and (18).

By substituting the parameter decompositions (see Eqs. (1*a*)–(1*c*)) into the energy equation and time averaging it, we obtain

$$\frac{\partial \bar{T}}{\partial t} + \bar{\vec{v}}_{nf} \cdot \nabla \bar{T} + \overline{\vec{v}'_{nf} \cdot \nabla T'} = \nabla \left(\frac{k_{nf}}{(\rho c_p)_{nf}} \right) \cdot \nabla \bar{T} + \frac{k_{nf}}{(\rho c_p)_{nf}} \nabla^2 (\bar{T}) + \frac{\bar{\Phi}}{(\rho c_p)_{nf}} \quad (25)$$

In general, we need to determine expressions for $\bar{T}$, T', $\bar{\vec{v}}_{nf}$, and $\vec{v}'_{nf}$ to derive an equation for the effective thermal conductivity, k_{nf}, for nanofluids. While $\bar{\vec{v}}_{nf}$ can be obtained from the momentum equation and continuity equation, $\bar{T}$ is the solution of the energy equation. Additionally, $\vec{v}'_{nf}$ can be calculated by combining Eqs. (10) and (24).

5 Reduced Governing Equations

To simplify the solution procedure, we assume that a temperature difference occurs only in the y-direction (see Figs. 2 and 3). In order to compare the new theory to batch-type measurements of nanofluids, it is also assumed that the average velocity of the mixture flow is equal to zero. Thus, performing fluid package analysis in 1D with linearized temperature profile, $\bar{\vec{v}}_{nf}$ and $\bar{T}$ are given as

$$\bar{\vec{v}}_{nf} = 0 \quad (26a)$$

$$\bar{T} = T^L + \frac{T^H - T^L}{R_c} y \quad (26b)$$

In any case, Eqs. (26*a*) and (26*b*) are based on the assumption that the thermal conductivity of fluids does not change with the heat-transfer mode. Thus, the new theory is valid for thermal conduction applications as well as for solving convective heat-transfer problems, recalling that thermal convection is thermal conduction of a moving fluid.

5.1 Energy Equation. We only focused on the micromixing part of the thermal conductivity of nanofluids. By incorporating all the assumptions made, the energy equation (25) can now be reduced to

$$\overline{\left| v_{nf}^{(y)'} \right| \frac{\partial T'}{\partial y}} = \frac{1}{(\rho c_p)_{nf}} \frac{\partial k_{mm}}{\partial y} \frac{\partial \bar{T}}{\partial y} \quad (27)$$

where $v_{nf}^{(y)'}$ is obtained from Eqs. (4*a*)–(4*c*) without the part induced by the motion of base-fluid molecules.

5.2 Extended Langevin Equation. Assuming only two nanoparticles interacting, Eq. (24) can be rewritten with $v'_p = \frac{dh}{dt}$ as

$$\frac{d^2 h}{dt^2} + \frac{3\pi d_p \mu_{bf}}{m_p} \frac{dh}{dt} + \left(\frac{F_{LD} - F_{Rep}}{h \cdot m_p} \right) \cdot h = F_B(t) \quad (28)$$

where $h = H - d_p$ is the distance between two nanoparticles changing with time t (see Fig. 3).

The extended Langevin equation (28) actually describes a nonlinear, transient, forced vibration system with damping. For further approximation, we use a linear vibration system instead of the nonlinear system and thereby neglecting any particle coagulation effect. Now, Eq. (28) can be rewritten as

$$\frac{d^2 h}{dt^2} + \frac{3\pi d_p \mu_{bf}}{m_p} \frac{dh}{dt} + K_{P-P} \cdot \frac{h}{m_p} = \frac{F_B(t)}{m_p} \quad (29)$$

where $K_{p\text{-}p}$ is an "effective stiffness" constant, which relates to the intensity of interactions between nanoparticles. With no loss of generality, we extend the definition of $K_{p\text{-}p}$ from effective stiffness for two-nanoparticle interaction to multi-nanoparticle interactions (see Fig. 3). Furthermore, such transient forced vibration can be changed to damped vibration with prescribed initial velocities [23]. Thus, Eq. (29) can be changed to

$$\frac{d^2 h}{dt^2} + \frac{3\pi d_p \mu_{bf}}{m_p} \frac{dh}{dt} + \frac{K_{P-P}}{m_p} \cdot h = 0 \quad (30)$$

with initial conditions

$$h(0) = 0 \text{ and } \frac{dh(N \cdot \tau_p)}{dt} = \xi_N \sqrt{\frac{\kappa_B \bar{T}}{2 m_p}} \quad (N = 0, 1, 2...) \quad (31e \text{ and } f)$$

where ξ_N is a random number satisfying normal distribution. Two additional "vibration parameters" are defined as follows:

$$\zeta = \frac{3\pi d_p \mu_{bf}}{2 m_p \omega_n} \quad (32)$$

and

$$\omega_n = \sqrt{\frac{K_{P-P}}{m_p}} \quad (33)$$

where ζ is the effective damping ratio and ω_n is the effective natural frequency. One may notice that according to the power law for an interaction potential between particles [18], $K_{p\text{-}p}$ should be a function of temperature, volume fraction, particle diameter, and density as well as the magnitude of the Hamaker constant.

For $\zeta < 1$, the system is underdamped [23]; thus, for an n-time interval τ_p, the nanoparticle fluctuation velocity $\left| v'_p \right|$ can be written as

$$\left| v'_p \right| = \frac{dh(t)}{dt} = |\xi| \cdot \sqrt{\frac{\kappa_B \bar{T}}{2 m_p}} \cdot \frac{d}{dt} \times \left[\exp(-\zeta \omega_n t) \cdot \left(\frac{\exp\left(i\omega_n \sqrt{1-\zeta^2} t \right) - \exp\left(-i\omega_n \sqrt{1-\zeta^2} t \right)}{2i\omega_n \sqrt{1-\zeta^2}} \right) \right] \quad (34a)$$

For $\zeta > 1$, the system is overdamped [23], and $\left| v'_p \right|$ based on the solution of Eq. (30) can be expressed as

$$\left| v'_p \right| = \frac{dh(t)}{dt} = |\xi| \cdot \sqrt{\frac{\kappa_B \bar{T}}{2 m_p}} \cdot \frac{d}{dt} \left[\exp(-\zeta \omega_n t) \cdot \left(\frac{\exp\left(\omega_n \sqrt{\zeta^2 - 1} t \right) - \exp\left(-\omega_n \sqrt{\zeta^2 - 1} t \right)}{2\omega_n \sqrt{\zeta^2 - 1}} \right) \right] \quad (34b)$$

By combining both Eqs. (34*a*) and (34*b*), the fluctuation velocity of nanoparticles for $\zeta \neq 1$ can be written as

$$\left| v'_p \right| = \frac{dh(t)}{dt} = |\xi| \cdot \sqrt{\frac{\kappa_B \bar{T}}{2 m_p}} \cdot \frac{d}{dt} \left[\exp(-\zeta \omega_n t) \cdot \left(\frac{\exp\left(\omega_n \sqrt{\zeta^2 - 1} t \right) - \exp\left(-\omega_n \sqrt{\zeta^2 - 1} t \right)}{2\omega_n \sqrt{\zeta^2 - 1}} \right) \right] \quad (35)$$

Equation (35) is a realistic expression for $\left| v'_p \right|$. Specifically, the nanoparticle is excited by the random force with an initial velocity

at the beginning of each characteristic time interval (see first term); then, vibration and damping occur gradually due to the influences of the London dispersion force, electrostatic repulsion force, and damping force (i.e., Stokes force). As will be demonstrated, with the increase of the particle–particle interaction intensity $K_{p\text{-}p}$, when $0 < K_{p\text{-}p} < O(10)$, k_{mm} decreases monotonically. The reason is that at higher intensity $K_{p\text{-}p}$, a nanoparticle arrangement is less affected by Brownian motion, thereby limiting the micromixing effect on heat transfer.

5.3 The Relationship Between T' and $\overline{T}$. A relationship between fluctuation temperature T' with average temperature $\overline{T}$ can be expressed for the 1D case as

$$T' = \lambda \frac{\partial \overline{T}}{\partial y} \tag{36}$$

where the mixture parameter λ is conceptually analogous to the concept of mean-molecular spacing in microfluidics of liquids.

We assume that λ has the same length in all directions. The fluid package will conserve its temperature for this characteristic scale before being mixed with the surrounding fluid. Hence, considering the volume fraction, we can express λ for the nanofluid as

$$\lambda = \varphi\lambda_p + (1-\varphi)\lambda_{bf} \tag{37}$$

where λ_p is the mixing length for nanoparticles and λ_{bf} is the mean-molecular distance for base fluids (i.e., $\lambda_{bf} = 0.3\,\text{nm}$ for water). Additionally, λ_p can be written as the average fluctuation velocity times, the time-interval that the particle can maintain its velocity and motion direction; hence

$$\lambda_p = \sqrt{\frac{\kappa_B \overline{T}}{2m_p}} \cdot \tau_p = \sqrt{\frac{\kappa_B \overline{T}}{2m_p}} \cdot \frac{m_p}{3\pi\mu_{bf} d_p} \tag{38}$$

where τ_p is the characteristic time for particles and μ_{bf} is considered as a parameter independent of T when calculating Eq. (38).

6 Thermal Conductivity of Nanofluids

The key goal is to derive a usable expression for the thermal conductivity of nanofluids based on sound physical insight, i.e., first engineering principles and benchmark experimental data sets. Returning to Eq. (3), k_{nf} is composed of the base-fluid static part k_{bf} and the new micromixing part k_{mm}.

6.1 Expression for k_{mm}. By combining Eqs. (10) and (35), we obtain

$$\left|v_{nf}^{(y)'}\right| = \frac{3}{2}\varphi\left(\frac{3}{32}\pi\frac{R_c^2}{r_p^2} - \frac{3}{128}\pi\frac{H^2}{r_p^2} - \frac{3\pi}{256}\ln(R_c) - \frac{3\pi}{256}\ln 2\right)\cdot|\xi|\cdot\left(\sqrt{\frac{\kappa_B\overline{T}^H}{2m_p}} - \sqrt{\frac{\kappa_B\overline{T}^L}{2m_p}}\right)$$
$$\cdot\frac{d}{dt}\left[\exp(-\zeta\omega_n t)\left(\frac{\exp\left(\omega_n\sqrt{\zeta^2-1}t\right) - \exp\left(-\omega_n\sqrt{\zeta^2-1}t\right)}{2\omega_n\sqrt{\zeta^2-1}}\right)\right] \tag{39}$$

By substituting Eqs. (36) and (39) into the reduced energy equation (27), and assuming that the base-fluid's mean-molecular spacing λ_{bf} is independent of temperature, we obtain

$$\frac{1}{\tau_p}\int_0^{\tau_p}\left|v_{nf}^{(y)'}\right|dt\cdot\varphi\cdot\sqrt{\frac{\kappa_B}{2m_p}}\tau_p\cdot\sqrt{\frac{1}{\overline{T}}}\cdot\frac{\partial\overline{T}}{\partial y}(\rho c_p)_{nf} = \frac{\partial k_{mm}}{\partial y} \tag{40}$$

Hence, the expression of k_{mm} is

$$k_{mm} = |\xi|\left(\frac{9\pi R_c^2}{64\,r_p^2} - \frac{9\pi\,H^2}{256\,r_p^2} - \frac{9\pi}{512}\ln(R_c) - \frac{9\pi}{512}\ln 2\right)$$
$$\cdot\frac{\exp(-\zeta\omega_n\tau_p)\cdot\left(\exp\left(\omega_n\sqrt{\zeta^2-1}\tau_p\right) - \exp\left(-\omega_n\sqrt{\zeta^2-1}\tau_p\right)\right)}{2\omega_n\sqrt{\zeta^2-1}\cdot\tau_p}$$
$$\cdot\varphi^2\cdot\frac{\kappa_B\tau_p}{2m_p}\cdot\left(\overline{T}\ln\overline{T} - \overline{T}\right)\cdot(\rho c_p)_{nf} \tag{41}$$

where we take $|\xi| = 0.7979$ which is based on the normal distribution of the random number from $-x_0 \le \xi \le x_0$ where $\int_{-x_0}^{x_0} p(x)dx \approx 100\%$. Also, after examining the order of each term in the expression $\left(\frac{9\pi}{64}\frac{R_c^2}{r_p^2} - \frac{9\pi}{256}\frac{H^2}{r_p^2} - \frac{9\pi}{512}\ln(R_c) - \frac{9\pi}{512}\ln 2\right)$, the last three terms can be neglected compared to the first term since $\frac{R_c}{r_p} = 375$. Thus, we can further simplify and rewrite k_{mm} as

$$k_{mm} = 49500\cdot C_c\cdot(\rho c_p)_{nf}\cdot\varphi^2\cdot\frac{\kappa_B\tau_p}{2m_p}\cdot\left(\overline{T}\ln\overline{T} - \overline{T}\right)$$
$$\cdot\frac{\exp(-\zeta\omega_n\tau_p)\cdot\left(\exp\left(\omega_n\sqrt{\zeta^2-1}\tau_p\right) - \exp\left(-\omega_n\sqrt{\zeta^2-1}\tau_p\right)\right)}{2\omega_n\sqrt{\zeta^2-1}\tau_p} \tag{42a}$$

In Eq. (42*a*), the large number 49,500 results from the superposition of the induced multinanoparticle velocities impacting the fluid package. By introducing ζ, ω_n, and τ_p are determined by Eqs. (32), (33), and (15*a*), respectively, we simplify Eq. (42*a*) as

$$k_{mm} = 49500\cdot\frac{\kappa_B\tau_p}{2m_p}\cdot C_c\cdot(\rho c_p)_{nf}\cdot\varphi^2\cdot\left(\overline{T}\ln\overline{T} - \overline{T}\right)$$
$$\cdot\frac{\exp(-\zeta\omega_n\tau_p)\sinh\left(\sqrt{\frac{(3\pi\mu_{bf}d_p)^2}{4m_p^2} - \frac{K_{P-P}}{m_p}}\frac{m_p}{3\pi\mu_{bf}d_p}\right)}{\tau_p\sqrt{\frac{(3\pi\mu_{bf}d_p)^2}{4m_p^2} - \frac{K_{P-P}}{m_p}}} \tag{42b}$$

In Eqs. (42*a*) and (42*b*), ρ_{nf} and c_{pnf} are given as [24]

$$\rho_{nf} = \rho_p\varphi + \rho_{bf}(1-\varphi) \tag{43a}$$

$$c_{pnf} = (c_p)_p\rho_p\varphi + (c_p)_{bf}\rho_{bf}(1-\varphi) \tag{43b}$$

and C_c is a correlation factor which describe the superposition effect of multiparticle interactions on one nanoparticle and the correction for the capturing radius, where R_c was selected based on multiparticle interactions. Specifically, for water-based nanofluids $C_c \approx 38$ which is not an empirical parameter. It can be calculated by considering surrounding particle-interactions with different distances to the central particle in lattices.

6.2 Expression for k_{nf}. Based on the results presented in Sec. 5.1, the F-K model expresses k_{nf} as (see Eq. (3))

$$k_{nf} = k_{static} + k_{mm} \tag{44}$$

where k_{static} is [25]

$$k_{static} = \left(1 + \frac{3\left(\frac{k_p}{k_{bf}} - 1\right)\varphi}{\left(\frac{k_p}{k_{bf}} + 2\right) - \left(\frac{k_p}{k_{bf}} - 1\right)\varphi}\right) k_{bf} \tag{45}$$

while k_{mm} is now given by substituting $m_p = \frac{\pi d_p^3}{6}$ into Eq. (42*b*) as

$$k_{mm} = 49,500 \cdot \kappa_B \cdot (\rho c_p)_{nf} \cdot F(\varphi) \cdot Y(\overline{T}) \cdot S(K_{P-P}, \rho_p, d_p, \mu_{bf}) \tag{46}$$

In summary, the contributing mixture parameters are

$$\rho_{nf} = \rho_p \varphi + \rho_{bf}(1 - \varphi) \tag{47a}$$

$$c_{pnf} = (c_p)_p \rho_p \varphi + (c_p)_{bf} \rho_{bf}(1 - \varphi) \tag{47b}$$

$$F(\varphi, d_p) = \frac{\varphi^2 \tau_p}{2m_p} = \frac{\varphi^2}{6\pi\mu_{bf} d_p} \tag{47c}$$

$$Y(\overline{T}) = \overline{T} \ln \overline{T} - \overline{T} \tag{47d}$$

$$S(K_{P-P}, \rho_p, d_p, \mu_{bf}) = \frac{\exp(-\zeta\omega_n\tau_p)\sinh\left(\sqrt{\frac{(3\pi\mu_{bf}d_p)^2}{4m_p^2} - \frac{K_{P-P}}{m_p}\frac{m_p}{3\pi\mu_{bf}d_p}}\right)}{\tau_p\sqrt{\frac{(3\pi\mu_{bf}d_p)^2}{4m_p^2} - \frac{K_{P-P}}{m_p}}} \cdot C_c \tag{47e}$$

Specifically, $K_{p\text{-}p}$ indicates the intensity of interactions between nanoparticles, which needs to be determined for a given type of nanoparticle-and-liquid pairing, while $S(K_{P-P}, \rho_p, d_p, \mu_{bf})$ can be interpreted as an amplifying function due to particle interactions and Stokes force.

6.3 Dependence of Parameters in the F-K Model. Examining Eq. (46), it is apparent that k_{mm} is a function of base-fluid properties, nanoparticle properties, volume fraction, temperature, and intensity of interactions between nanoparticles. Specifically, k_{mm} is related to φ by approximately an order of 2 in the $F(\varphi, m_p)$ term and related to $\overline{T}$ by the order of 1 to 2 in $Y(\overline{T})$. Also, we can conclude that k_{mm} will increase when the mass of nanoparticles decreases. Considering nanoparticles of the same material, k_{mm} will increase when the diameter decreases (see the Stokes–Einstein equation). It should be noted that the effect on thermal conductivity due to nanoparticle-interaction is presented solely by the function $S(K_{P-P}, \rho_p, d_p, \mu_{bf})$. As $K_{p\text{-}p}$ increases, i.e., the interactions between nanoparticles are stronger, $S(K_{P-P}, \rho_p, d_p, \mu_{bf})$ decreases, leading to a lower enhancement in thermal conductivity. Such a relationship is physically reasonable because strong interactions limit nanoparticle-fluctuations reduce the micromixing effect on heat transfer. As part of $S(K_{P-P}, \rho_p, d_p, \mu_{bf})$, μ_{bf} indicates the intensity of the Stokes force exerted on the nanoparticle as a drag force.

The derivation of Eq. (41*b*) reveals that if we do not consider the interaction between nanoparticles and Stokes force, which means $|v_p'| = |\xi| \cdot \sqrt{\frac{\kappa_B \overline{T}}{2m_p}}$ instead of Eq. (35), a simplified expression for k_{mm} which is called $k_{Brownian}$, can be written as

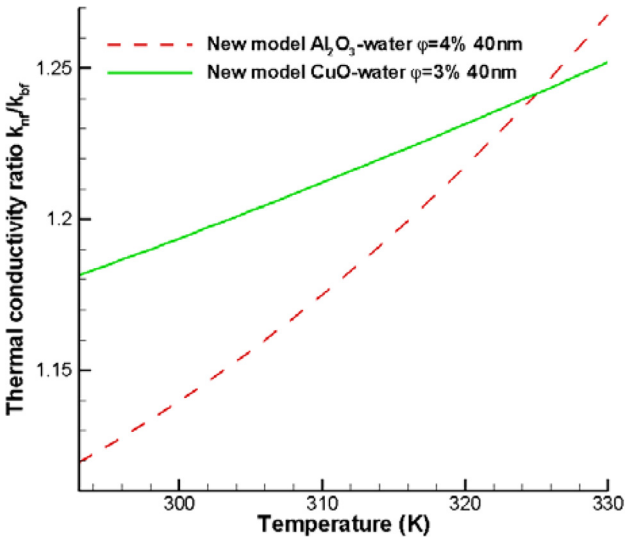

Fig. 6 F-K model predictions for nanofluids dependence on temperature

$$k_{Brownian} = 49,500 \cdot \frac{\kappa_B}{6\pi\mu_{bf}d_p} \cdot (\rho c_p)_{nf} \cdot \varphi^2 \cdot (\overline{T} \ln \overline{T} - \overline{T}) \tag{48}$$

Hence, Eq. (44) changes into

$$k_{nf} = k_{static} + k_{Brownian} \tag{49}$$

Further comparisons between the knf-expressions with and without particle–particle interactions are discussed in Sec. 6.3.3.

6.3.1 Dependence on Temperature. The dependence on temperature of the F-K model is best visualized by plotting Eq. (46). Two sample nanofluids are presented in Fig. 6, i.e., $\varphi = 4\%$ and $d_p = 40$ nm Al_2O_3-water nanofluid as well as $\varphi = 3\%$ and $d_p = 40$ nm CuO-water nanofluid. From Fig. 6, it is apparent that the thermal conductivity of nanofluids is a function of temperature of the order of 1 to 2. Also, the Al_2O_3-water nanofluid curve exhibits a larger slope (i.e., increasing trend) when compared to the CuO-water nanofluid. The thermal conductivity of CuO (32.9 W/mK) being close to the one of Al_2O_3 (35 W/mK), the slope difference between the two nanofluids is mainly due to the different volume fractions.

6.3.2 Dependence on Volume Fraction. The dependence of the F-K model on volume fraction is of the order of 1 to 2, which is justifiable because we assumed that $K_{p\text{-}p}$ is not a function of volume fraction. Such a relationship indicates that the relationship between thermal conductivity of nanofluids and the volume fraction is *nonlinear,* which is different from the (linear) relationship in the classical models [25,26].

6.3.3 Dependence on Particle–Particle Interaction Intensity. The effect of volume fraction on $K_{p\text{-}p}$ can be expressed in terms of temperature and particle properties. Clearly, when the temperature increases, particles submerged in a liquid are more activated, which indicates that $K_{p\text{-}p}$ decreases when the temperature increases. Also, $K_{p\text{-}p}$ being related to the particle mass, $K_{p\text{-}p}$ will increase when the particle diameter increases. As a result, $K_{p\text{-}p}$ expressions change for different nanoparticle suspensions and different temperatures. Additionally, although presently C_c is assumed to be constant, it varies with the type of nanoparticle-liquid pairing.

By comparing Eqs. (45) and (47*e*), it can be concluded that the particle–particle interaction and Stokes force act as an amplifier to the micro–mixing effect caused by Brownian motion of nanoparticles. The amplification factor is $S(K_{P-P}, \rho_p, d_p, \mu_{bf})$

given as Eq. (46*e*). Generally, the magnitude of $K_{p\text{-}p}$ can be written as

$$K_{P-P} = \rho_p \cdot \sqrt{d_p} \cdot \left(\frac{32.1724 \cdot 273\,K}{T} - 19.4849 \right) \tag{50}$$

Clearly, for Eq. (50) to be valid, T must be less than 370 K (or 97 °C) to avoid phase-change (at p_{atm}), which is the case for most nanofluid flow applications. Furthermore, this temperature restriction is due to the mathematical linear simplification of the extended Langevin equation. One should notice that Eq. (50) is only suitable for nanoparticles suspended in water, because $K_{p\text{-}p}$ is related to the Hamaker constant A, which varies with the type of base fluid as the medium between particles.

7 Comparisons

We compared Eq. (49) with benchmark experimental data sets [26–31] which include different nanoparticles, i.e., Al_2O_3, CuO, TiO_2, and ZrO_2, and different base fluids, i.e., water, ethylene glycol, and engine oil, for different volume fractions, temperatures, and particle diameters. Additionally, more recently presented experimental data for nanofluid thermal conductivities were also investigated [32].

7.1 Comparisons With Benchmark Experimental Data

7.1.1 Al_2O_3-Water Nanofluid Comparisons. The comparison with Al_2O_3-water nanofluids features a range of particle-diameter from 29 nm to 47 nm, volume fractions from 0% to 8%, and temperatures from 294 K to 330 K, by taking the intensity of interactions, $K_{p\text{-}p}$, in the form of Eq. (50).

The results are shown in Figs. 7 and 8. The F-K model predictions match well with most of the experimental data. However, our predictions do not show a good agreement for 36 nm Al_2O_3-water nanofluid with 6% volume fraction when compared to experimental data by Mintsa et al. [32]. However, our simulation results match experimental data sets by Li and Peterson [3] as well as Chon et al. [30], who employed the same Al_2O_3-water nanofluid but with lower volume fraction (4% versus 6%) and higher particle diameter (i.e., 47 nm versus 36 nm), respectively. Thus, it appears that the difference between our prediction and Mintsa's experimental data is due to experimental errors. In conclusion, the F-K model provides good predictions for Al_2O_3-water nanofluids with volume fractions less than 8%.

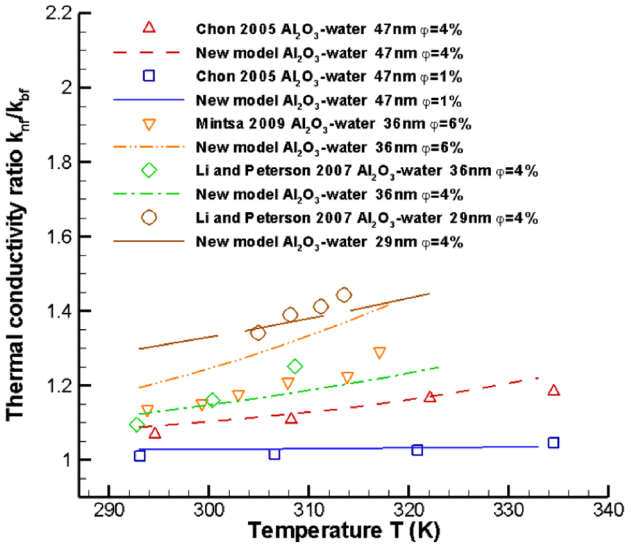

Fig. 8 Comparisons between F-K model and benchmark experimental data for Al_2O_3-water nanofluids dependence on temperature T

7.1.2 CuO-Water Nanofluid Comparisons. For the comparison with CuO-water nanofluids, two temperatures, i.e., T = 294 K and 309 K, were considered (see Fig. 9). The F-K model shows a good agreement with the experimental data when the volume fraction φ is between 3% and 4.5%. As expected, k_{nf}/k_{bf} is higher at elevated temperatures. Curiously, the measurements by Das et al. [29] indicate the volume fraction has hardly any effect on the nanofluid thermal conductivity. This disagreement between F-K model and the experimental data of Das et al. [29] at low volume fractions, i.e., $\varphi < 3\%$, is partly because the experimental data are unreasonably high for nanofluids at low volume fractions. Specifically, a linear curve fit of Das data [29] will provide k_{nf}/k_{bf}-values larger than one as φ approaches zero, which is unacceptable. As an aside, while Mintsa et al. [32] did not show any significant k_{nf}/k_{bf}-dependence on volume fraction either, Eastman et al. [33] had measured increased k_{nf}-values over 50% for $\varphi = 5\%$.

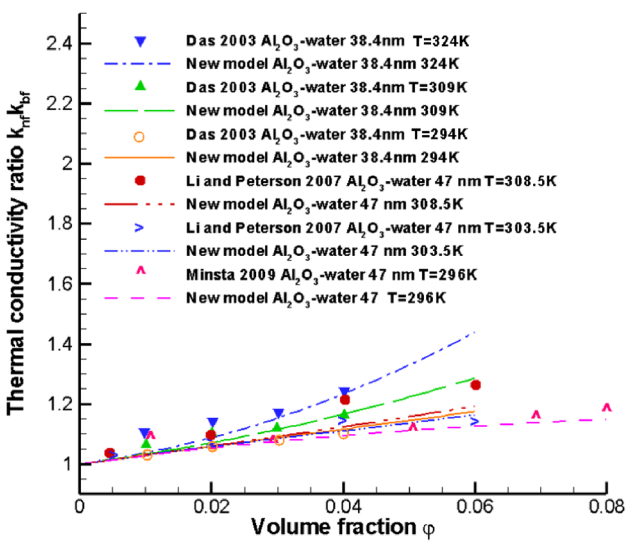

Fig. 7 Comparisons between F-K model and benchmark experimental data for Al_2O_3-water nanofluids dependence on volume fraction φ

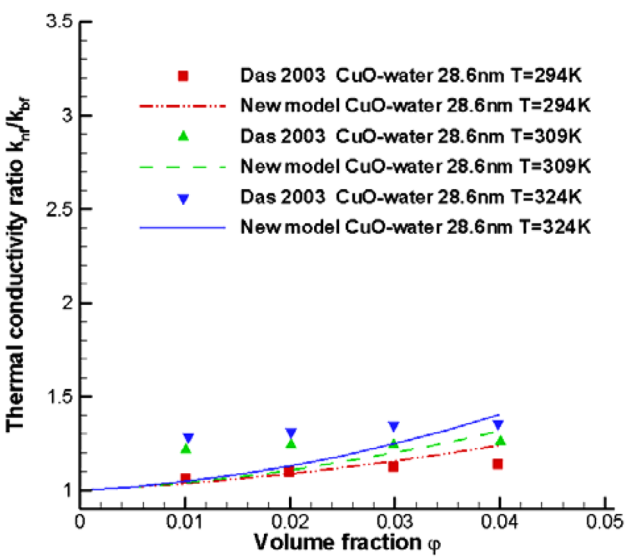

Fig. 9 Comparisons between F-K model and benchmark experimental data for CuO-water nanofluids dependence on volume fraction φ

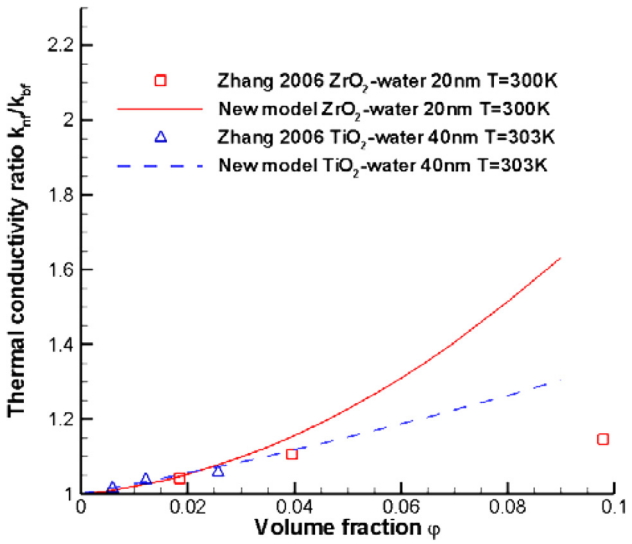

Fig. 10 Comparisons between F-K model and benchmark experimental data for ZrO_2-water and TiO_2-water nanofluids dependence on volume fraction φ

7.1.3 Other Metal-Oxide Comparisons. As general cases, we chose ZrO_2-water and TiO_2-water nanofluids. The results are shown in Fig. 10. At volume fractions lower than 4%, the F-K model shows a good match with the experimental data [31]. However, for higher volume fractions, i.e., $\varphi > 4\%$, our model indicates a faster increase in thermal conductivity than the experimental data. This may be because in experimental settings the effect of Brownian motion on k_{nf} at higher volume fractions could be limited, while in our model micromixing continues with the increase in volume fraction. Clearly, adjustment of the magnitude of C_c could correct that phenomenon if proven to be valid. It should be also noted that the restrictions of parameter ranges are coupled to the expression for $K_{P\text{-}P}$.

7.2 Comparisons With Other k_{nf}-Models. The MSB model of Prasher [11] and the model of Bao [12] have been compared with the new theory in light of experimental data sets (see Figs. 10 and 12), while the performance of the KKL model is depicted in Fig. 1. Additional background information and a discussion of the pros and cons of the KKL and MSB models are given by Li [24].

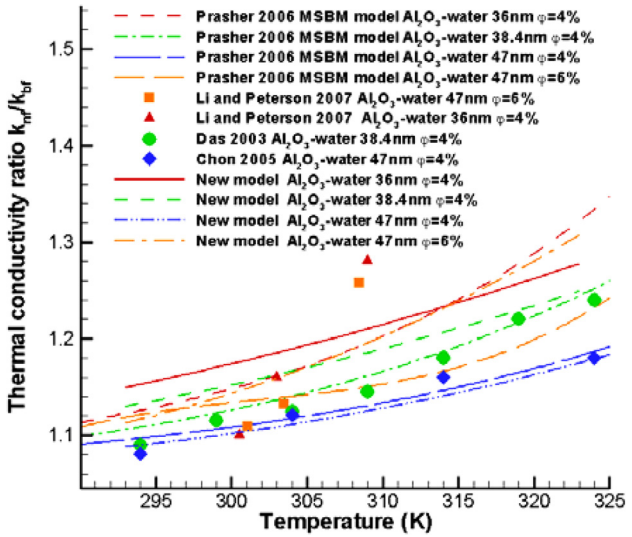

Fig. 11 Comparisons between F-K model and MSB model [11]

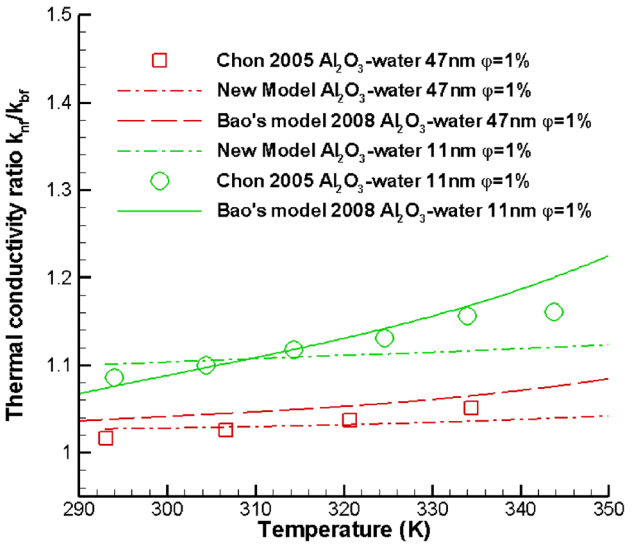

Fig. 12 Comparisons between F-K model and Bao's model [12]

As indicated in Fig. 11, the trends of the new theory and the MSB model are similar for different nanofluids and show good agreements with the observations by Chon et al. [30]. However, the F-K model predicts in most cases higher thermal conductivities than the MSB model. As discussed by Li [24], the MSB model contains two major data-matching coefficients, which lack physical explanations. Figure 12 shows comparable agreements between Bao's model and the F-K model in light of the experimental data by Chon et al. [30]. However, the theory proposed by Li [24] does not include particle–particle interaction and involves a velocity-correlation function, R(t), to evaluate the nanoparticle relaxation time that carries an adjustment parameter M.

8 Limitations

The theory (F-K model) is derived based on several assumptions:

- During each characteristic time interval of Brownian motion, the initial velocity magnitude is generated randomly; thus, it can be assumed that the surrounding fluid is at pseudo-steady-state. Specifically, the response time for a nanoparticle ($\sim 6 \times 10^{-2}$ ns) in a fluid is much smaller than the required time for a nanoparticle to move a distance of, say, its diameter (~6 ns). Hence, a steady-state Stokes solution for the velocity field can be applied.
- The capturing radius (see Sec. 2.3.1) is calculated based on the 99.8% criterion in order to encapsulate the multiparticle Brownian-motion effect. Such a criterion indicates that for particles at the position $r > r_c$, the particle velocity is too small to have an impact on the centered nanofluid velocity.

The F-K model matches experimental data best for several types of spherical metal-oxide nanoparticles ($20 < d_p < 50$ nm) in water with volume fractions up to 5%, and mixture temperatures below 350 K.

9 Summary

This is the first of a two-part paper which proposes a new theory explaining the experimentally observed enhancement of the thermal conductivity, k_{nf}, of nanofluids (Part I). It provides the derivation of the F-K model as well as comparisons with benchmark experimental data sets and other theories, focusing mainly on aluminum and copper oxide nanoparticles in water. The new thermal conductivity expression consists of a base-fluid static part, k_{bf}, and a new "micromixing" part, k_{mm}, i.e., $k_{nf} = k_{bf} + k_{mm}$.

While k_{bf} relies on Maxwell's theory, k_{mm} encapsulates nanoparticle characteristics and liquid properties as well as Brownian-motion induced nanoparticle fluctuations, nanoparticle volume fractions, mixture-temperature changes, particle–particle interactions, and random temperature fluctuations causing liquid-particle interactions. Thus, fundamental physics principles include the Brownian-motion effect, an extended Langevin equation with scaled interaction forces, and a turbulence-inspired heat transfer equation.

The F-K model matches experimental data for several types of metal-oxide nanoparticles ($20 < d_p < 50$ nm) in water with volume fractions up to 5%, and mixture temperatures below 350 K. The new theory can be readily extended to accommodate other forms of nanoparticle-liquid pairings and to include non-spherical nanomaterial. While other recent models match selectively experimental k_{nf} data sets as well but employ unexplained matching parameters, the F-K theory is solidly based on physical principles.

References

[1] Das, S. K., Choi, S. U. S., Yu, W., and Pradeep, T., 2008, *Nanofluids: Science and Technology*, John Wiley & Sons, New York.

[2] Tillman, P., and Hill. J. M., 2007, "Determination of Nanolayer Thickness for a Nanofluid," Int. Commun. Heat Mass Transfer, **34**(4), pp. 399–407.

[3] Li, C. H., and Peterson, G. P., 2007, "Mixing Effect on the Enhancement of the Effective Thermal Conductivity of Nanoparticle Suspensions (Nanofluids)," Int. J. Heat Mass Transfer, **50**, pp. 4668–4677.

[4] Keblinski, P., Phillpot, S. R., Choi, S. U. S., and Eastman, J. A., 2002, "Mechanisms of Heat Flow in Suspensions of Nano-Seized Particles (Nanofluids)," Int. J. Heat Mass Transfer, **45**, pp. 855–863.

[5] Koo, J., and Kleinstreuer, C., 2004, "A New Thermal Conductivity Model for Nanofluids," J. Nanopart. Res., **6**, pp. 577–588.

[6] Kleinstreuer, C., and Li, J., 2008, "Discussion: Effects of Various Parameters on Nanofluid Thermal Conductivity," ASME J. Heat Transfer, **130**, p. 025501.

[7] Gupte, S. K., and Advani, S. G., 1995, "Role of Micro-Convection Due to Non-Affine Motion of Particles in a Mono-Disperse Suspension," Int. J. Heat Mass Transfer, **38**(16), pp. 2945–2958.

[8] Leal, L. G., 1973, "On the Effective Conductivity of a Dilute Suspension of Spherical Drops in the Limit of Low Particle Peclet Number," Chem. Eng. Commun., **1**, pp. 21–31.

[9] Gupte, S. K., Advani, S. G., and Hu, P., 1993, "A Cell Model to Investigate the Influence of Fall Velocity Distribution on Transport Processes in a Sedimenting Suspension," 64th Annual Society of Rheology Meeting, Santa Barbara, CA.

[10] Wang, X. W., Xu, X. F., and Choi, S. U. S., 1999, "Thermal Conductivity of Nanoparticle-Fluid Mixture," J. Thermophys. Heat Transfer, **13**, pp. 474–480.

[11] Prasher, R., 2006, "Brownian-Motion-Based Convective-Conductive Model for the Effective Thermal Conductivity of Nanofluids," ASME J. Heat Transfer, **128**, pp. 588–595.

[12] Bao, Y., 2009, "Thermal Conductivity Equations Based on Brownian Motion in Suspensions of Nanoparticles (Nanofluids)," ASME J. Heat Transfer, **130**, p. 042408.

[13] Kaviany, M., 1995, *Principles of Heat Transfer in Porous Media*, Springer-Verlag, Berlin, Germany.

[14] Xuan, Y., and Roetzel, W., 2000, "Conceptions for Heat Transfer Correlation of Nanofluids," Int. J. Heat Mass Transfer, **43**, pp. 3701–3707.

[15] Panton, R. L., 2005, *Incompressible Flow*, 3rd ed., John Wiley & Sons, New York.

[16] Koo, J. M., 2005, "Computational Nanofluid Flow and Heat Transfer Analyses Applied to Micro-Systems," Ph.D. Dissertation, NC State University, Raleigh, NC.

[17] Einstein, A., 1956, *Investigations on the Theory of the Brownian Movement*, Dover Publications, Inc., New York.

[18] Israelachvili, J. N., 1985, *Intermolecular and Surface Forces With Applications to Colloidal and Biological Systems*, Academic Press, Inc., Orlando, FL.

[19] Wang, X. W., and Xu, X. F., 1999, "Thermal Conductivity of Nanoparticle-Fluid Mixture," J. Thermophys. Heat Transfer, **13**, pp. 474–480.

[20] Feng, Y., and Lin, J. Z., 2008, "The Collision Efficiency of Spherical Dioctyl Phthalate Aerosol Particles in the Brownian Coagulation," Chin. Phys. B, **17**(12), pp. 4547–4553.

[21] Ratnesh, K. S., 2008, "Effect of Brownian Motion on Thermal Conductivity of Nanofluids," ASME J. Heat Transfer, **130**, p. 042406.

[22] Karniadakis, G. E., 2002, *Micro Flows Fundamentals and Simulation*, Springer-Verlag, New York.

[23] Benaroya, H., 1998, *Mechanical Vibration: Analysis, Uncertainties, and Control*, Simon & Schuster/Viacom Company, Upper Saddle River, NJ.

[24] Li, J., 2008, "Computational Analysis of Nanofluid Flow in Microchannels With Applications to Micro-Heat Sinks and Bio-MEMS," Ph.D. dissertation, North Carolina State University, Raleigh, NC.

[25] Maxwell, J. C., 1891, *A Treatise on Electricity and Magnetism*, 3rd ed., Clarendon Press, Oxford, UK.

[26] Hamilton, R. L., and Crosser, O. K., 1962, "Thermal Conductivity of Heterogeneous Two Component Systems," Ind. Eng. Chem. Fundam., **1**, pp. 187–191.

[27] Xuan, Y., and Li, Q., 2000, "Heat Transfer Enhancement of Nanofluids," Int. J. Heat Mass Transfer, **21**, pp. 58–64.

[28] Xie, H., Wang, J., Xi, T., and Liu, Y., 2002, "Thermal Conductivity of Suspensions Containing Nanosized SiC Particles," Int. J. Thermophys., **23**(2), pp. 571–580.

[29] Das, S. K., Putra, N., Theisen, P., and Roetzel, W., 2003, "Temperature Dependence of Thermal Conductivity Enhancement for Nanofluids," ASME J. Heat Transfer, **125**, pp. 567–574.

[30] Chon, C. H., Kihm, K. D., Lee, S. P., and Choi, S. U. S., 2005, "Empirical Correlation Finding the Role of Temperature and Particle Size for Nanofluid (Al_2O_3) Thermal Conductivity Enhancement," Appl. Phys. Lett., **87**, p. 153107.

[31] Zhang, X., Gu, H., and Fujii, M., 2006, "Experimental Study on the Effective Thermal Conductivity and Thermal Diffusivity of Nanofluid," AIAA J., **41**, pp. 831–840.

[32] Mintsa, H. A., Roy, G., Nguyen, C. T., and Doucet, D., 2009, "New Temperature Dependent Thermal Conductivity Data for Water-Based Nanofluids," Int. J. Therm. Sci., **48**, pp. 363–371.

[33] Eastman, J. A., Choi, U. S., Li, S., Thompson, L. J., and Lee, S., 1997, "Enhanced Thermal Conductivity Through the Development of Nanofluids," *Nanophase and Nanocomposite Materials II*, S. Komarneni, J. C. Parker, and H. J. Wollenberger, eds., MRS, Pittsburg, PA, pp. 3–11.

[34] Hunter, R. J., 1991, *Foundations of Colloid Science*, Vol. I, Oxford University Press Inc., New York.